**Smart Structures and Systems**, *Vol. 15, No. 6 (2015) 1463-1479*
DOI: http://dx.doi.org/10.12989/sss.2015.15.6.1463 

# On time reversal-based signal enhancement for active lamb wave-based damage identification

Qiang Wang*[1], Shenfang Yuan[2], Ming Hong[3] and Zhongqing Su[3,4]

[1]*School of Automation, Nanjing University of Posts and Telecommunications, 9 Wen Yuan Road, Nanjing, P.R. China, 210046*
[2]*The Aeronautical Science Key Laboratory for Smart Materials and Structures, Nanjing University of Aeronautics and Astronautics, 29 Yu Dao Street, Nanjing, P.R. China, 210016*
[3]*Department of Mechanical Engineering, The Hong Kong Polytechnic University, Kowloon, Hong Kong SAR*
[4]*The Hong Kong Polytechnic University Shenzhen Research Institute, 18 Yue Xing Road, Shenzhen, P.R. China, 518057*

*(Received October 26, 2013, Revised March 2, 2014, Accepted March 10, 2014)*

**Abstract.** Lamb waves have been a promising candidate for quantitative damage identification for various engineering structures, taking advantage of their superb capabilities of traveling for long distances with fast propagation and low attenuation. However, the application of Lamb waves in damage identification so far has been hampered by the fact that the characteristic signals associated with defects are generally weaker compared with those arising from boundary reflections, mode conversions and environmental noises, making it a tough task to achieve satisfactory damage identification from the time series. With awareness of this challenge, this paper proposes a time reversal-based technique to enhance the strength of damage-scattered signals, which has been previously applied to bulk wave-based damage detection successfully. The investigation includes (i) an analysis of Lamb wave propagation in a plate, generated by PZT patches mounted on the structure; (ii) an introduction of the time reversal theory dedicated for waveform reconstruction with a narrow-band input; (iii) a process of enhancing damage-scattered signals based on time reversal focalization; and (iv) the experimental investigation of the proposed approach to enhance the damage identification on a composite plate. The results have demonstrated that signals scattered by delamination in the composite plate can be enhanced remarkably with the assistance of the proposed process, benefiting from which the damage in the plate is identified with ease and high precision.

**Keywords:** time reversal; damage detection; Lamb waves; signal focalization; imaging damage

## 1. Introduction

Composite materials have been increasingly used in many engineering structures, including aircraft, automobiles and ships, thanks to their high strength-to-weight and stiffness-to-weight ratios. Monitoring the intergrity and reliability of composite structures is thereofore of great significance. However, damage in composite structures can be very complicated, multiform, and usually invisible, posing a challenge on damage analysis and identification. Without periodic

*Corresponding author, Associate Professor, E-mail: wangqiang@njupt.edu.cn


http://www.techno-press.org/?journal=sss&subpage=8 ISSN: 1738-1584 (Print), 1738-1991 (Online)

assessment and maintenance, the damage could potentially lead to catastrophic failure of the structure. To detect damage in composite structures, traditional nondestructive testing (NDT) methods have apparent limitations due to their intrinsic natures of high cost, time consumption, complicated manipulation, and point-by-point measurement (which makes it difficult in monitoring structures of large dimensions). On the other hand, Lamb wave-based damage detection techniques provide a promising solution to damage identification in composites with their attractive features of cost-effectiveness, quick investigation, high sensitivity to damage, ease of manipulation, and the ability to monitor structures of large areas (Yuan *et al.* 2003, Giurgiutiu 2000, Boller 2000).

As one of the most effective damage detection techniques, Lamb wave-based active diagnosis approach is attracting increasing attention of researchers and engineers. However, the prevalence of such an approach has been impeded by the complexity of the analysis and interpretation of Lamb wave modes due to their dispersive and multimodal natures, as well as the low energy of characteristic signals associated with defects. Allowing for this, most research efforts have been dedicated to extracting damage-scattered signals by comparing monitored signals with baseline data. Nevertheless, such a process may introduce unsolicited errors and suffer from low signal-to-noise radios (SNR) of the signals of interest, because the signals containing damage information are usually much weaker than the rest.

With awareness of those drawbacks, and in an effort to enhance the energetic strength of characteristic signals pertinent to defects, this paper proposes a time reversal-based technique, which has been investigated and implemented in a number of areas, including ultrasonic imaging (Draeger *et al.* 1997, Ing and Fink 1998), underwater acoustic imaging, NDT (Bardos and Fink 2002, Fink 1999, Jeong 2009), and wireless communications (Song *et al.* 2006). The time reversal technique has been applied to compensate for the dispersion of Lamb waves, and improve the SNR of captured signals (Ing and Fink 1998, Bardos and Fink 2002, Fink 1999, Gangadharan *et al.* 2009, Jeong 2009, Ratneshwar and Ryan 2009, Zhang *et al.* 2010, Wang *et al.* 2004, Fink and Lewiner 2000), with concentrations on the reconstruction or refocusing of excitation signals. Although it has been employed successfully in a number of ultrasonic wave based detection methods (Bardos and Fink 2002, Fink 1999), reports of applying time reversal to improve the performance of defect-scattered Lamb wave signals are not common, largely due to the fact that the acquisition of focalized scattered signals can become very challenging, thanks to the complicated characteristics of Lamb waves. In recognition of such a dilemma, the proposed method in this paper aims to resolve this problem by enhancing the recognizability of damage scattered Lamb waves, and improve the practicality of baseline-dependent damage detection methods.

In this study, a time reversal-based signal enhancing method is presented to strengthen the damage-scattered waves, hence to improve identification results, which is organized as follows: (i) an analysis of the propagation of Lamb waves generated by PZT patches mounted on a plate is described in Section 2; (ii) in Section 3, a signal amplification method based on the time reversal theory is investigated to focus and enhance the scattered signals, and a damage imaging approach is also addressed; and (iii) experimental investigations are presented in Section 4 to demonstrate the validity of the proposed method.

## 2. Time reversal process of lamb waves using PZT arrays

### *2.1 Lamb waves in a plate*

Lamb waves are a kind of elastic waves propagating in plate- or shell-like structures. Unlike bulk waves, the use of Lamb waves is complicated due to their dispersive and multimodal features (Ing and Fink 1998). Theoretically, these two features can be investigated by solving the Rayleigh–Lamb equations defined by the symmetrical and anti-symmetrical modes on an infinite plate with a thickness denoted by 2*h* (Ing and Fink 1998)

$$\left(k^2+s^2\right)^2\cosh(qh)\sinh(sh)-4k^2qs\sinh(qh)\cosh(sh)=0 \tag{1a}$$

$$\left(k^2+s^2\right)^2\sinh(qh)\cosh(sh)-4k^2qs\cosh(qh)\sinh(sh)=0 \tag{1b}$$

where $q^2=k^2-k_l^2$ and $s^2=k^2-k_t^2$. Furthermore, $k$ denotes the wave number, and $k_l$ and $k_t$ are the wave numbers for the longitudinal and shear modes, respectively. The dispersion curves can be determined by solving Eqs. (1(a)) and (l(b)), and expressed in terms of the frequency-thickness product versus the group velocity $C_g$, which is defined as

$$C_g=\frac{d\omega}{dk} \tag{2}$$

where $\omega$ denotes the angular frequency. For a plate with a constant thickness, the dispersion curve can be represented as a function of the frequency. The dispersive nature of Lamb waves causes the different frequency components of Lamb waves to travel in the plate at different speeds, thus altering the shape of the wave packet. It should be noted that multiple wave modes can be extracted from Eq. (1). The symmetric modes are designated $S_0$, $S_1$, $S_2$, *etc.*, while the antisymmetric are designated $A_0$, $A_1$, $A_2$, *etc*.

The exact solution to Lamb wave propagation can be quite complex. Consider a homogeneous, isotropic elastic plate, as shown in Fig. 1, on which wo PZT patches are attached with one serving as an actuator ($P_1$) and the other as a sensor ($P_2$). The response voltage at $P_2$ can be represented as

$$V_{P_2}(r,\omega)=K_{P_2}(\omega)\hat{E}_{P_2}(r,\omega) \tag{3}$$

where $r$, $V_{P_2}$, $K_{P_2}$ and $\hat{E}_{P_2}$ are the wave propagation distance from the center of $P_1$ to that of $P_2$, the response voltage at $P_2$, the electro-mechanical efficiency constant and the surface strain at the center of $P_2$ with respect to the angular frequency $\omega$, respectively. Here, the surface strain was assumed uniform, which, at $P_2$, can be rewritten as

$$\hat{E}_{P_2}(r,\omega)=\hat{I}(\omega)K_{P_1}(\omega)G_{12}(r,\omega) \tag{4}$$

where $\hat{I}$, $K_{P_1}$ and $G_{12}$ are the input voltage at $P_1$, the electro-mechanical efficiency constant of $P_1$ with respect to angular frequency $\omega$, and the frequency response function, respectively. The frequency response function $G_{12}$ is complicated, and is usually analyzed with Green function (Wang *et al.* 2004, Park *et al.* 2009). Xu and Giurgiutiu (2007) and Yu *et al.* (2010) have developed a theoretical model for the analysis of PZT active sensor related to Lamb wave excitation and transmission. To make the presentation straightforward and easy to understand, $G_{12}$ is simplified based on this theoretical model, and can be written as (Xu and Giurgiutiu 2007)

$$G_{12}(r,\omega)=\sum_{A_n} a_{A_n}^{12}(r,\omega)e^{-jk_{A_n}r}+\sum_{S_n} a_{S_n}^{12}(r,\omega)e^{-jk_{S_n}r}, k_{A_n}=\frac{\omega}{c_{A_n}}, k_{S_n}=\frac{\omega}{c_{S_n}} \quad (5)$$

where $a_{A_n}^{12}(r,\omega)$, $k_{A_n}$, $c_{A_n}$ are respectively the amplitude, wave number and velocity of $A_n$ mode, and $a_{S_n}^{12}(r,\omega)$, $k_{S_n}$, $c_{S_n}$ are the corresponding counterparts of $S_n$ mode. From the Eq. (5), we can find that $G_{12}$ is dependent on the frequency ($\omega$) and the wave numbers ($k_{A_n}$ and $k_{S_n}$). Because the wave number is a function of the density, flexural stiffness and thickness of the plate, the wave propagation characteristics described in Eq. (5) depend on the fundamental properties of the plate.

### 2.2 Time reversal process

Similar to the time reversal mirror for ultrasonics (Fink and Lewiner 2000), Lamb waves sensed by several different sensors with a single actuation can be focused at the source by performing a time reversal process as shown in Fig. 2, while the original input signal also can be rebuilt in the process. In such a case, several PZT patches attached to a plate-like structure are used to configure a sensor array, with one of them serving as an actuator ($P_A$) and the others as sensors ($P_i$, $i$ =1, 2, 3…). After collecting all the Lamb wave responses to the input signal $\boldsymbol{I}$ at $P_A$, the following steps are performed in the time reversal process.

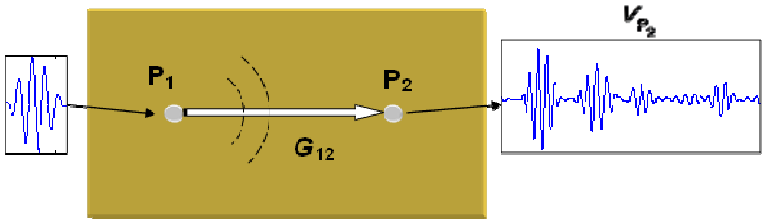


Fig. 1 Lamb wave propagation in a plate

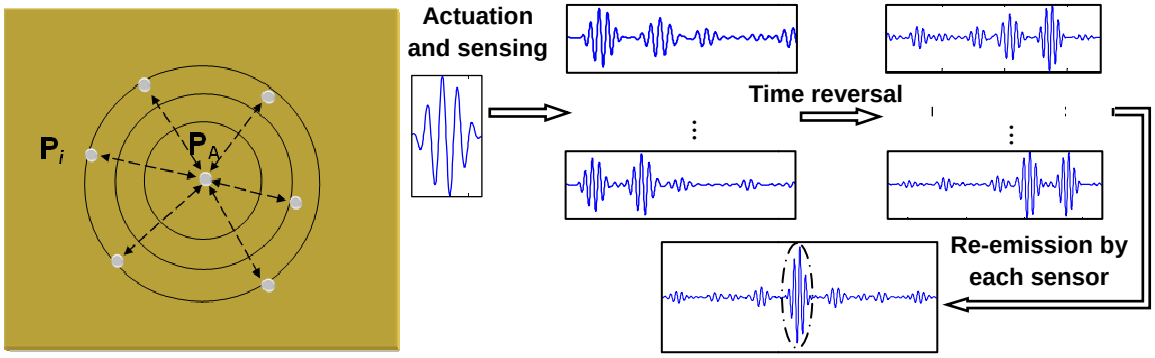


Fig. 2 A typical time reversal process

(1) Time-reverse the collected response signals $V_{\mathrm{P}i}$ which was presented in Eqs. (3) and (4). Note that the time reversal operation on the response signal at P*i* is equivalent to taking the complex conjugate in the frequency domain:

$$\hat{V}^*_{\mathrm{P}i}(r_i,\omega)=K^*_{\mathrm{P}i}\hat{E}^*_{\mathrm{P}i}(r_i,\omega) \tag{6}$$

where the asterisk denotes the complex conjugate, $r_i$ , $V_{\mathrm{P}i}$ , $K_{\mathrm{P}i}$ and $\hat{E}_{\mathrm{P}i}$ are the wave propagation distance from the center of $\mathrm{P_A}$ to that of $\mathrm{P}_i$, the response voltage at $\mathrm{P}_i$, the electro-mechanical efficiency constant and the surface strain at the center of $\mathrm{P}_i$ with respect to angular frequency $\omega$, respectively.

(2) Re-emit the time-reversed signal $\hat{V}^*_{Pi}$ at $\mathrm{P_i}$ and collect the response at $\mathrm{P_A}$. The response can be represented in a similar fashion as in Eq. (3)

$$\hat{V}_{\mathrm{P_A}}(r,\omega)=K_{\mathrm{P_A}}\hat{E}_{\mathrm{P_A}}(\omega) \tag{7}$$

where

$$\hat{E}_{P_{\mathrm{A}}}(\omega)=\sum_i \hat{V}^*_{Pi}(r_i,\omega)K_{Pi}(\omega)G_{Ai}(r_i,\omega) \tag{8}$$

$G_{Ai}$ is the frequency response function of P*i* with a similar form as in Eq. (5). Combining Eqs. (4), (6) and (8), Eq. (7) can be rewritten as (Wang *et al.* 2004, Park *et al*. 2009, Yu *et al.* 2010)

$$\hat{V}_{\mathrm{P_A}}(\omega)=\hat{I}^*(\omega)\sum_i K^*_{\mathrm{P_A}}(\omega)K^*_{\mathrm{P}_i}(\omega)K_{\mathrm{P_A}}(\omega)K_{\mathrm{P}_i}(\omega)G_{Ai}(r_i,\omega)G^*_{Ai}(r_i,\omega) \tag{9}$$

Performing an inverse Fourier transform, the refocused input signal $V_A$ at $\mathrm{P}_A$ is

$$\hat{V}_{\mathrm{P_A}}(t)=\frac{1}{2\pi}\int_{-\infty}^{\infty}\hat{I}^*(\omega)\sum_i K^*_{Ai}(\omega)K_{Ai}(\omega)G_{Ai}(r_i,\omega)G^*_{Ai}(r_i,\omega)\mathrm{e}^{-j\omega t}d\omega \tag{10}$$

where $K_{Ai}$ denotes the product of $K_{\mathrm{P_A}}$ and $K_{\mathrm{P}i}$. When only the $A_0$ and $S_0$ modes exist in the structure,

$$\begin{aligned}
&G_{Ai}(r_i,\omega)G^*_{Ai}(r_i,\omega)\\
&=\left(a^{Ai}_{A_0}(r_i,\omega)e^{-jk_Ar_i}+a^{Ai}_{S_0}(r_i,\omega)e^{-jk_Sr_i}\right)\left[\left(a^{Ai}_{A_0}(r_i,\omega)\right)^*e^{jk_Ar_i}+\left(a^{Ai}_{S_0}(r_i,\omega)\right)^*e^{jk_Sr_i}\right]\\
&=\left|a^{Ai}_{A_0}(r_i,\omega)\right|^2+\left|a^{Ai}_{S_0}(r_i,\omega)\right|^2+a^{Ai}_{A_0}(r_i,\omega)\left(a^{Ai}_{S_0}(r_i,\omega)\right)^*e^{-j(k_A-k_S)r_i}\\
&\quad+\left[a^{Ai}_{A_0}(r_i,\omega)\left(a^{Ai}_{S_0}(r_i,\omega)\right)^*e^{-j(k_A-k_S)r_i}\right]^*
\end{aligned} \tag{11}$$

In Eq. (11), the term $\left|a^{Ai}_{A_0}(r_i,\omega)\right|^2+\left|a^{Ai}_{S_0}(r_i,\omega)\right|^2$ indicates that the dispersion is compensated because both $a^{Ai}_{A_0}(r_i,\omega)$ and $a^{Ai}_{S_0}(r_i,\omega)$ are amplitudes without phase and time information, namely there is no phase between them, and different Lamb wave modes arrive at the actuator

simultaneously. Thus, there exists a cumulative term $\sum_i \left( \left| a_{A_0}^{Ai}(r_i,\omega) \right|^2 + \left| a_{S_0}^{Ai}(r_i,\omega) \right|^2 \right)$ in Eq. (10), the focalization of all the amplitudes from different sensors, which should be significantly greater than others as shown in Fig. 2(b). It also can be learned that more sensors result in more significant focalization. Meanwhile, it should be noted that the onset of each captured signal must be uniform and synchronized to the input waveform.

Wang *et al.* (2004) has experimentally validated this process with both broadband and narrowband input signals, and achieved apparent focalization and good compensation for the dispersion of Lamb waves. However, in the context of time reversal applications for Lamb waves, it is found that the time-reversed results are considerably complicated under the broadband input, as a result of abundant frequency components in the captured signals. In Eqs. (10) and (11), when the number of sensor is limited, the exact reconstruction of the original excitation $\hat{I}$ is achieved only if $K_{Ai}^*(\omega)K_{Ai}(\omega)$ and $G_{Ai}(r,\omega)G_{Ai}^*(r,\omega)$ are independent of the angular frequency $\omega$ (Wang *et al.* 2004, Park *et al.* 2009, Yu *et al.* 2010). Consequently, the original input signal cannot be properly reconstructed if a broadband input signal is used (Wang *et al.* 2004). In fact, a reconstruction of simple waveforms (i.e., narrowband inputs) can instead be advantageous in the subsequent signal analysis and processing, especially for damage detection, because the process transforms complicated structural responses into simple ones. By choosing a narrowband input waveform at a specific frequency, the independence of the angular frequency $\omega$ is approximated, with limited Lamb wave modes excited in the structure. Thus, $K$ becomes constant. The frequency response function $G$ is simplified and only determined by the distance $r$. Eqs. (10) and (11) can be rewritten as

$$\hat{V}_{\mathrm{P_A}}(t) = \frac{1}{2\pi}\int_{-\infty}^{\infty} \hat{I}^*(\omega) \sum_i K_{Ai}^2 G_{Ai}^*(r_i) G_{Ai}(r_i) \mathrm{e}^{-j\omega t} d\omega \tag{12}$$

$$G_{Ai}^*(r_i)G_{Ai}(r_i) = \left| a_{A_0}^{Ai}(r_i) \right|^2 + \left| a_{S_0}^{Ai}(r_i) \right|^2 + a_{A_0}^{Ai}(r_i) a_{S_0}^{Ai}(r_i) e^{\pm j(k_A - k_S)r_i} \tag{13}$$

Solving Eq. (12) yields

$$\hat{V}_{\mathrm{P_A}}(t) = \sum_i \frac{K_{Ai}^2}{2\pi} \left\{ \left( \left| a_{A_0}^{Ai}(r_i) \right|^2 + \left| a_{S_0}^{Ai}(r_i) \right|^2 \right) \hat{I}(-t) + a_{A_0}^{Ai}(r_i) a_{S_0}^{Ai}(r_i) \hat{I}\left[ -t \pm \left( r_i/c_{A_0} - r_i/c_{S_0} \right) \right] \right\} \tag{14}$$

It can be seen that $\hat{V}_{\mathrm{P_A}}(t)$ is composed of a main lobe at zero time and symmetrical sides at the time of $\pm\left( r_i/c_{A_0} - r_i/c_{S_0} \right)$, with the main lobe dominating the whole domain. Such dominance becomes more intensive if more Lamb modes are involved. As a result, the main lobe $\sum_i \frac{K_{Ai}^2}{2\pi} \left( \left| a_{A_0}^{Ai}(r_i) \right|^2 + \left| a_{S_0}^{Ai}(r_i) \right|^2 \right) \hat{I}(-t)$ can be considered as the focusing of different modes and the exact reconstruction of the original excitation $\hat{I}$. Here, it should be noted that the time resolution of the signals may decrease when a narrow-band input signal is excited.

For the sake of signal interpretation and processing, it is preferred to generate a single Lamb mode in practice. Xu and Giurgiutiu (2007) and Yu *et al.* (2010) discussed the single mode tuning effects on the propagation of Lamb waves generated by PZT sensors, and discovered that the

normalized amplitude of each mode under the excitation of PZT wafers followed the general pattern of a sine function, which hit zeros when the half length of the PZT sensor equaled an odd multiple of one of the wave numbers of the Lamb waves. Thus, using smoothed tone-burst excitation at the carrier frequency $f_c$ and frequency tuning, it is possible to confine the excitation to a particular Lamb wave mode. Eq. (14) can be further simplified as follows, if only $A_0$ is generated

$$\hat{V}_{\mathrm{P_A}}(t) = \hat{I}(-t)\sum_{i=2}^{N}\frac{K_{Ai}^2\left|a_{A_0}^{Ai}(r_i)\right|^2}{2\pi} = \hat{I}(-t)\sum_i K_i \quad (i=1,2,3,\cdots) \tag{15}$$

The discussion above indicates that the time reversal process should be helpful for signal analysis and simplify the applications of Lamb waves. In the next section, an improved damage detection methodology will be further discussed based on the time reversal process of Lamb waves.

## 3. Improved damage detection using Lamb waves

### *3.1 Time reversal enhancement of damage scattered lamb waves*

In the context of Lamb wave-based active diagnosis, damage is deemed as a wave source to emit scattering signals to sensors. By collecting those signals and applying certain algorithms, the damage can be visually detected via imaging (Zhang *et al.* 2010, Wang *et al.* 2004). However, Lamb wave propagations and the frequency response function $G$ are complicated due to wave reflections at boundaries and mode conversions in practice, with which damage-scattered signals are usually inundated. As a result, it becomes difficult to discriminate the damage scattered signals from other disturbances, impairing Lamb wave-based damage detection.

With such awareness, there is an increasing attention to adopt the time reversal technique to enhance damage-scattered signals. The theory can be simply depicted in the following steps: (i) the damage is first considered as the wave source to generate scattering waves; (ii) the captured signals at each sensor is time-reversed; and (iii) the time-reversed signals are re-emitted from the sensors. Hence, all the waves scattered by the damage can be finally focalized at the damage and accordingly enhanced. On the other hand, signals from reflections and mode conversions cannot be focalized during the time reversal process and would finally counteract each other, since these waves do not have a uniform and common source to enable the focalization. Following the above discussion, the time reversal enhancing process can be expressed below.

(1) For a given tone-burst at a certain center frequency, the difference between the acquired signals before and after the introduction of damage can be considered as the damage-scattered signal. As already addressed, the merits of using narrowband input waveforms are threefold: (1) the independence of the angular frequency $\omega$, (2) the electro-mechanical efficiency constant of the PZT sensors remains unchanged (Wang *et al.* 2004, Park *et al.* 2009, Yu *et al.* 2010), and (3) a dominant wave mode, such as $A_0$ mode, exists at the certain center frequency, making the frequency response function and the signal process straightforward. Considering a PZT patch $P_i$ serving as the actuator, a tone-burst at a certain center frequency is generated, similar to Eqs. (4) and (14), the incidence (single Lamb mode) upon the damage is

$$D_i = I \cdot K_{\mathrm{P}_i} \cdot G_{\mathrm{P}_i\mathrm{D}}(r_i) = I \cdot K_{\mathrm{P}_i} \cdot a_{A_0}(r_i) e^{-jk_{A_0} r_i} \quad (i = 1, 2, 3...) \tag{16}$$

where $D_i$ is the amplitude of the wave mode arriving at the damage caused by the excitation of $\mathrm{P}_i$, $G_{\mathrm{P}_i\mathrm{D}}(r_i)$ is the frequency response function, and $r_i$ is the distance between $\mathrm{P}_i$ and the damage. Therefore, the signals sensed by the PZT $\mathrm{P}_k$ can be written as

$$\hat{V}_{ik} = D_i \cdot G_{\mathrm{DP}_k}(r_k) \cdot K_{\mathrm{P}_k} = D_i \cdot K_{\mathrm{P}_k} \cdot a_{A_0}(r_k) e^{-jk_{A_0} r_k}, \quad i, k = 1, 2, 3... \; i \neq k \tag{17}$$

where, similar to Eq. (16), $G_{\mathrm{P}_k\mathrm{D}}(r_k)$ is the frequency response function, and $r_k$ is the distance between the sensor (PZT $k$) and the damage.

(2) Time-reversed and re-emitted signal at each PZT sensor is focalized at the damage (Wang *et al.* 2004). By Eqs. (9), (15) and (17), the focused wave at the damage can be expressed as

$$\begin{aligned} D_i' &= \sum_k \hat{V}_{ik}^* \cdot a_{A_0}(r_k) e^{-jk_{A_0} r_k} \cdot K_{\mathrm{P}_k} = D_i^* \cdot \sum_k a_{A_0}(r_k) e^{-jk_{A_0} r_k} \cdot K_{\mathrm{P}_k} \cdot \left( a_{A_0}(r_k) e^{-jk_{A_0} r_k} \cdot K_{\mathrm{P}_k} \right)^* \\ &= D_i^*(\omega) \cdot \sum_k \left| a_{A_0}(r_k) \cdot K_{\mathrm{P}_k} \right|^2 \end{aligned} \tag{18}$$

Comparing Eq. (18) with Eq. (16), an accumulated coefficient can be noticed in Eq. (18), *i.e.*, $\sum_k \left| a_{A_0}(r_k) \cdot K_{\mathrm{P}_k} \right|^2$, which is the focalization of the sensing signals at the damage. As a result of amplification, the amplitude or power of the focused wave $D_i'$ is greater than that of the wave $D_i$, which is achieved without applying the time reversal focalization. It also can be seen that the focalized wave is not the original input signal $I$, but instead the wave $D_i$. Thus, if multi-modes are excited, they all exist in the focalized wave. However, it is difficult to choose the characteristic mode related to the damage in the re-scattering waves, which is also one of the reasons why narrowband input signal for single mode excitation is adopted in this study as mentioned earlier.

Note again that the damage-scattered signals recorded by the sensors are of greater amplitude than that of the signals collected without the time reversal procedure. Combining Eqs. (16) and (18), the amplified scattering signals collected by PZT $\mathrm{P}_l$ can be obtained as

$$\begin{aligned} \hat{V}_{il}^E &= a_{A_0}(r_l) e^{-jk_{A_0} r_l} \cdot K_{\mathrm{P}_l} \cdot D_i^*(\omega) \cdot \sum_k \left| a_{A_0}(r_k) \cdot K_{\mathrm{P}_k} \right|^2 \\ &= I^* \cdot \sum_k \left( a_{A_0}(r_i) e^{-jk_{A_0} r_i} \cdot K_{\mathrm{P}_i} \cdot a_{A_0}(r_k) e^{-jk_{A_0} r_k} \cdot K_{\mathrm{P}_k} \right)^* \\ &\quad \cdot \left( a_{A_0}(r_k) e^{-jk_{A_0} r_k} \cdot K_{\mathrm{P}_k} \cdot a_{A_0}(r_l) e^{-jk_{A_0} r_l} \cdot K_{\mathrm{P}_l} \right) \quad i, k, l = 1, 2, 3... \; i \neq l \neq k \end{aligned} \tag{19}$$

Such a process can be achieved conveniently in ultrasonic nondestructive testing (Fink and Lewiner 2000). However, aimed at Lamb wave-based damage detection for plate-like structures, the amplification of damage-scattered waves are difficult to be obtained by traditional techniques. Figure 3 shows the time reversal process of the damage-scattered waves in a plate by traditional equipment. In this situation, PZT sensors and actuators are bonded on the surface of the plate so

that the sensor (e.g., $P_l$ in Fig. 3) receives the amplified damage-scattered waves (dotted line in Fig. 3) and the waves directly from the actuators (solid lines in Fig. 3) synchronously, resulting in an overlapped signal.

Here a signal processing technique is proposed to realize the amplification of damage-scattered signals. In Eq. (19), the term $\left(a_{A_0}(r_i)e^{-jk_{A_0}r_i}\cdot K_{P_i}\cdot a_{A_0}(r_k)e^{-jk_{A_0}r_k}\cdot K_{P_k}\right)$ denotes the transfer function of the scattering signals from $P_i$ to $P_k$. The term $\left(a_{A_0}(r_k)e^{-jk_{A_0}r_k}\cdot K_{P_k}\cdot a_{A_0}(r_l)e^{-jk_{A_0}r_l}\cdot K_{P_l}\right)$ denotes the transfer function from $P_k$ to $P_l$. If these transfer functions are known beforehand, the amplified signals can be calculated by Eq. (19). Obviously, all those equations are only correlative with the damage-scattered signals, which can be obtained easily using traditional equipment. However, it is difficult to directly model these transfer functions due to the dispersive and multimodal natures of Lamb waves. To resolve such a problem, the unknown transfer functions are replaced by known damage-scattered signals. Following the above derivation, and by multiplying both sides of the Eq. (19) with the input wave *I*, Eq. (19) can be re-written as

$$\begin{aligned}\widehat{V}'^{E}_{il} &= \widehat{V}^{E}_{il}\cdot I \\ &= \sum_k \left(I\cdot a_{A_0}(r_i)e^{-jk_{A_0}r_i}\cdot K_{P_i}\cdot a_{A_0}(r_k)e^{-jk_{A_0}r_k}\cdot K_{P_k}\right)^* \\ &\quad\cdot\left(I\cdot a_{A_0}(r_k)e^{-jk_{A_0}r_k}\cdot K_{P_k}\cdot a_{A_0}(r_l)e^{-jk_{A_0}r_l}\cdot K_{P_l}\right) \\ &= \sum_k \widehat{V}^{*}_{ik}\cdot\widehat{V}_{kl}\end{aligned} \tag{20}$$

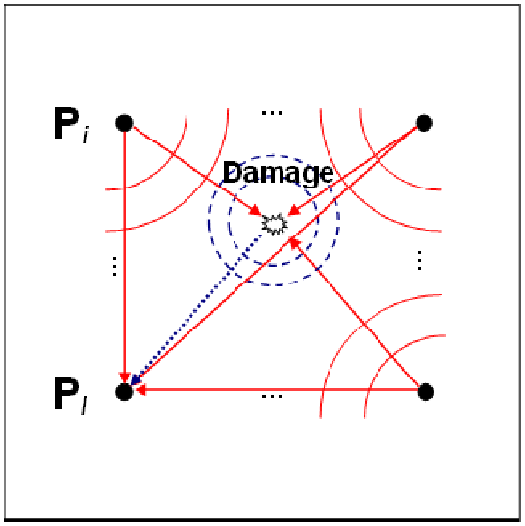


Fig. 3 Time reversal process of damage–scattered waves in a plate using traditional equipment

where $\widehat{V}_{ik}$ and $\widehat{V}_{kl}$ are the damage-scattered signal sensed by $P_k$ ($P_i$ acts as the actuator) and $P_l$ ($P_k$ acts as the actuator), respectively. The asterisk means time reversal in the time domain. These scattering signals were obtained in step (i) (Section 3). Actually, $\widehat{V}_{il}'^{E}$ is the amplified damage-scattered signal under the input wave $I^* \cdot I$ which has the same frequency characteristics as those of the signal *I*. As a result, such a process does not change the velocities of Lamb waves and the arrivals of the damage-scattered signals sensed by the PZT sensors, and transfer functions are not required any more.

### *3.2 Time-reversal-based imaging approach*

Consider a distributed PZT array consisting of *N* active actuators/sensors bonded in the monitored area. It is assumed that $t_0$ is the time when the damage-scattered waves come forth, and $t_w$ is the final time of the sensing signals. The signals captured by each sensor are intercepted by a time window from $t_0$ to $t_w$. Consequently, the time-reversed and re-emitted signals are inversely fed into the same PZT element. With such a process, the focalization of the waves at the damage can be achieved with the captured signals of an enhanced SNR, facilitating damage identification. With the damage-scattered signals, the damage can be visualized by virtue of an imaging technique by relating the contrast at a particular pixel (or focal point) in an image to the amplitude of the amplified scattering signal received by every sensor in the sensor network (Zhang *et al.* 2010, Wang *et al.* 2004). The contrast *S* at a particular location or imaging pixel (*i*, *j*) can be expressed as

$$S(i,j) = \max\left[\sum_{m=1}^{N} a_m f_m\left(t - t_{mij}\right)\right] \tag{21}$$

where $t_{mij} = \dfrac{R_{mij}}{c_g}$ and $a_m = \dfrac{1}{\max\limits_m |f_m|}$. $f_m(t)$ denotes the amplified scattering signal captured by sensor $P_m$, $t_0$ is the time when damage scatters the signals, $t_{mij}$ is the propagation time of the Lamb wave from the sensor *m* to the pixel (*i*, *j*) in the image, $R_{mij}$ designates the distance between $P_m$ and the pixel $S(i, j)$, $c_g$ is the group velocity of the collected signal in the structure, and $a_m$ refers to the appropriate aperture weighting to each sensor, which compensates for the amplitude differences among different sensors. All the notations can be seen in Fig. 4.

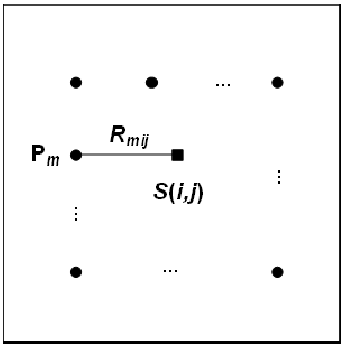


Fig. 4 Notations for time-reversal-based imaging approach

## 4. Experiments

A quasi-isotropic glass-reinforced epoxy composite plate (800×800×2 $mm^3$) was ultrasonically examined as shown in Fig. 5. A delamination with a diameter of circa 20 mm was introduced to the plate at (50 mm, 102 mm) using a hammer, as shown in Fig. 5(a). Five piezoelectric elements, 8 mm in diameter and 0.48 mm in thickness, were permanently attached to the plate, forming a sensor network. Positions of all the PZT sensors in the plate are listed in Table 1. A PZT scanning and damage diagnostic system was designed to generate and collect the signals (Qiu and Yuan 2009), as illustrated in Fig. 5(c). In this experiment, a five-cycle Hanning-windowed sine burst at a center frequency of 40 kHz was excited. The generated Lamb waves are representatively shown in Fig. 6 with $A_0$ dominating the whole domain. The sensing signals were sampled by the diagnostic system at a sampling rate of 5 MHz.

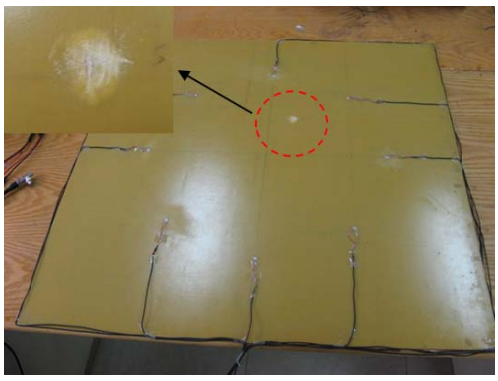

(a) Quasi-isotropic epoxy glass-reinforced composite plate with PZT array

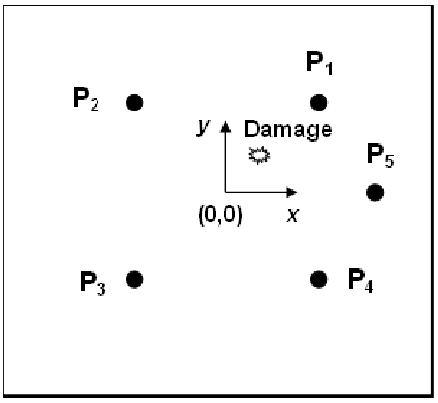


(b) Locations of the PZTs within the sensor network

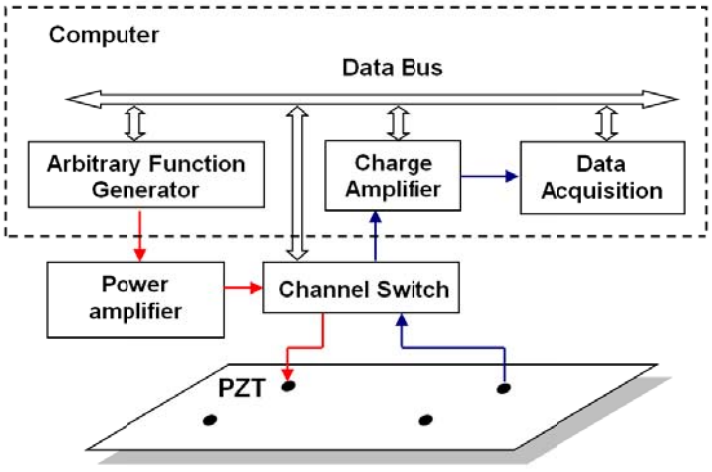


(c) PZT scanning and damage diagnostic system

Fig. 5 Experimental set-up

Table 1 PZT sensor coordinates

| PZT | Coordinates ($x$, $y$) [mm] |
|---|---|
| $P_1$ | (177, 177) |
| $P_2$ | (-177, 177) |
| $P_3$ | (-177, -177) |
| $P_4$ | (177, -177) |
| $P_5$ | (250, 0) |

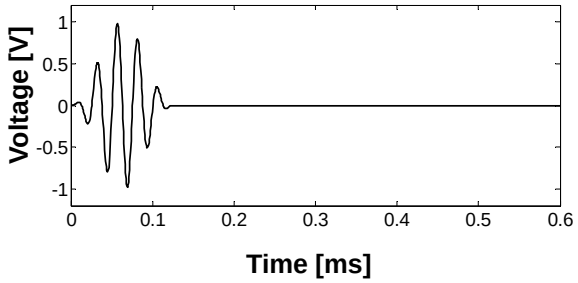


Fig. 6 The excitation waveform (Wang *et al.* 2004, Park *et al.* 2009)

As shown in Fig. 5(b), five PZTs are collocated in four quadrants. If one PZT serves as an actuator, the others as sensors, there are 16 actuator-sensor pairs in total, corresponding to 16 captured signals. Fig. 7(a) shows the damage-scattered signals in the time domain captured by PZTs P2–P5 when P1 acted as the actuator, respectively named $f_{12}$, $f_{13}$, $f_{14}$ and $f_{15}$ in time domain, and $\widehat{V}_{12}$, $\widehat{V}_{13}$, $\widehat{V}_{14}$ and $\widehat{V}_{15}$ in the frequency domain as indicated in Eq. (17) - Eq. (20). Fig. 7(b) shows the corresponding envelopes of the captured signals in the time domain. Because of their short distance to the actuator and damage, the damage-scattered waves received by $P_2$ and $P_5$ were of strong energy and well observable, as can be seen in Fig. 7. However, those sensed by $P_3$ and $P_4$ were of small amplitude due to their relative large distance from the damage and actuator. The maximum peaks appear at other times as shown in Fig. 7(b), and error may be introduced when these signals are used. Figure 8 presents the damage identification image based on the signals from Fig. 7. It can be seen that there is no visible focalization at the damage (as indicated by the red circle), but rather at scattered points, presenting improper identification results.

With the time reversal process, the damage-scattered signals captured by each actuator-sensor pair can be enhanced. For example, the enhanced signal $\widehat{V}_{12}'^{E}$ in the frequency domain at $P_2$ is

$$\widehat{V}_{12}'^{E} = \widehat{V}_{13}^{*} \cdot \widehat{V}_{32} + \widehat{V}_{14}^{*} \cdot \widehat{V}_{42} + \widehat{V}_{15}^{*} \cdot \widehat{V}_{52} \tag{22}$$

Fig. 9 shows the time reversal enforcing process of each signal from Fig. 7. Amplified signals in the time domain are named $f'_{12}$, $f'_{13}$, $f'_{14}$ and $f'_{15}$, and their counterparts in frequency domain are $\widehat{V}_{12}'^{E}$, $\widehat{V}_{13}'^{E}$, $\widehat{V}_{14}'^{E}$ and $\widehat{V}_{15}'^{E}$, respectively, as expressed in Eq. (20). The denotation $s$ in Fig. 9 refers to the enhanced signal $f'_{1k}$, and $s1$, $s2$, $s3$ refer to the accumulation parts as expressed in Eqs. (20) and (22). Here, it should be noted that the scattering point around the damage may vary from one sensor to another. Meanwhile, the wavelengths of the excited waves are small, so that the

phase difference caused by this problem is not negligible in the time reversal process. Destructive superposition may happen when the damage-scattered signals are used directly. Thus, envelopes of the signals are time-reversed and superimposed to realize the focalization, because the length of the wave packet is as five times long as the wavelength, and the influence of the phase difference becomes limited and negligible. The superposition of signal envelopes are displayed in Fig. 9, with one main peak much higher than others in each focalized signal.

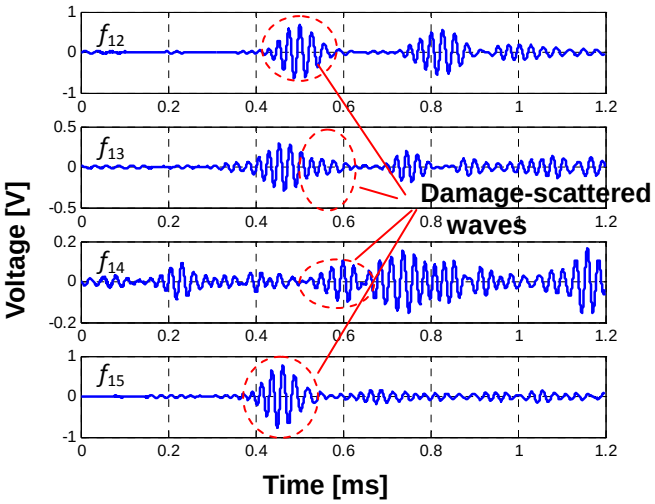


(a) Damage scattering waves sensed by PZT $P_2$, $P_3$, $P_4$ and $P_5$

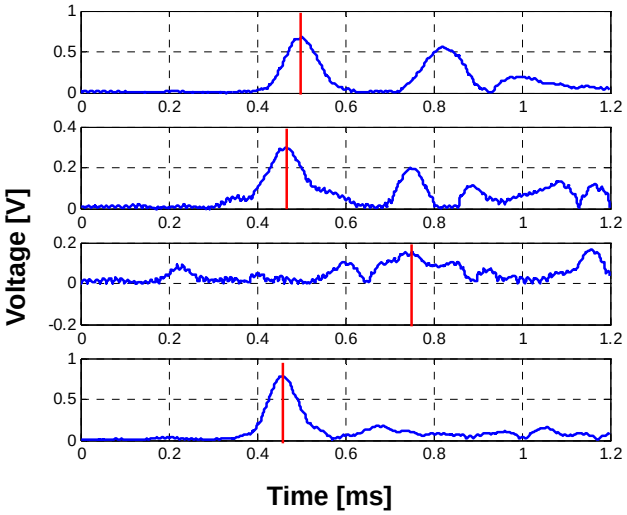


(b) Envelopes of signals sensed by PZT $P_2$, $P_3$, $P_4$ and $P_5$

Fig. 7 Damage scattering waves and their envelopes sensed by PZT $P_2$, $P_3$, $P_4$ and $P_5$

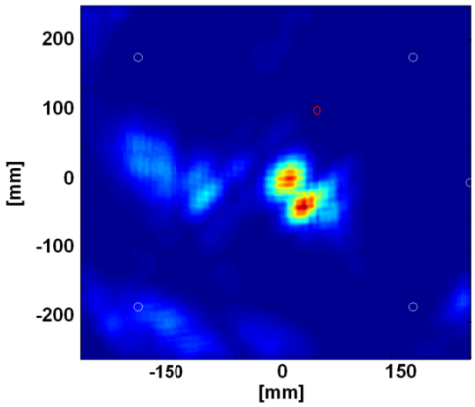


Fig. 8 Damage imaging results by the signals shown in Fig. 5 (white circles indicate the PZT sensors, and the red one is the actual damage center)

Because the specimen (i.e., the glass-enforced epoxy plate) used in this study is quasi-isotropic, the group velocities of Lamb waves in this material can be regarded as a constant. Using time reversal imaging method, the damage was well detected as displayed in Fig. 10. To illustrate the location of the damage more clearly, this image can be improved with a threshold value set as a percentage of the maximum value of the whole image so that irrelevant information, such as noise, can be filtered. Fig. 11 shows the result with a preset threshold of 80%.

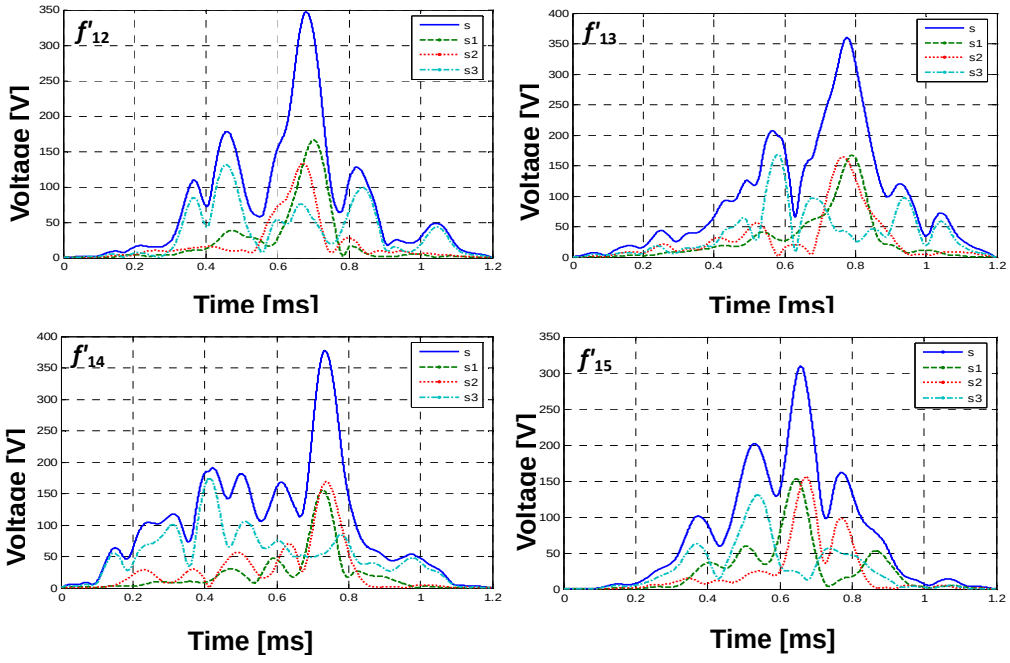


Fig. 9 The time reversal enforcing process to each signal (***s*=*s*1+*s*2+*s*3**)

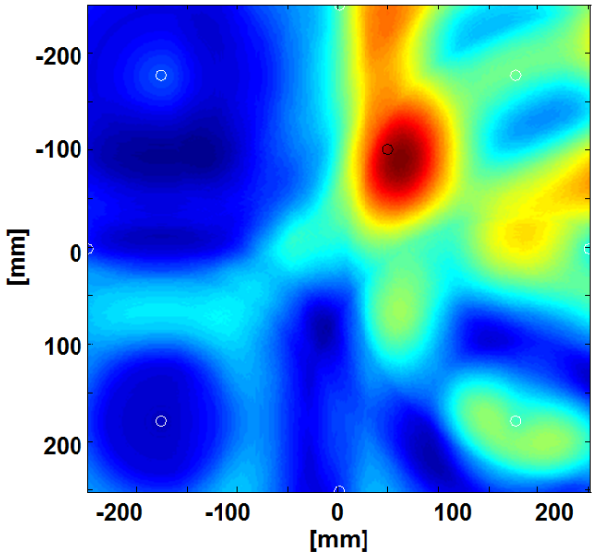


Fig. 10 Damage detection result (white circles indicate the PZT sensors, and the black one is the damage center)

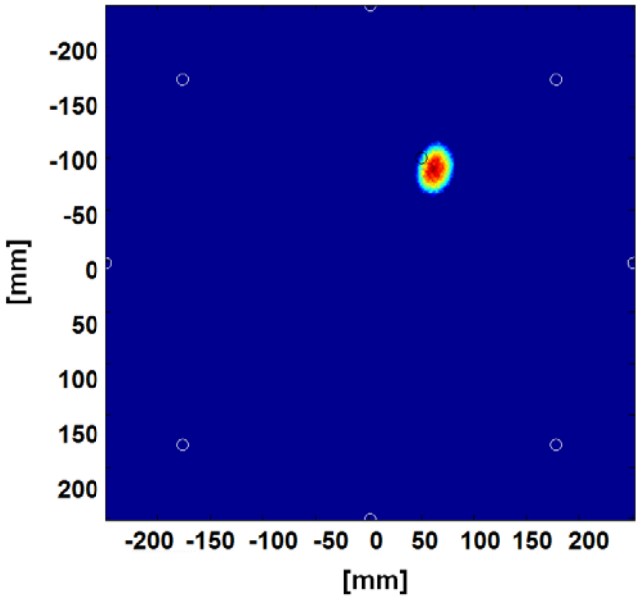


Fig. 11 Improved image by applying a threshold value to the image in Fig. 10

## 5. Conclusions

In this paper, a damage detection and imaging method based on time-reversal enhanced Lamb waves was proposed for identifying damage in a composite plate. First, the propagation characteristics of Lamb waves in a plate as well as the corresponding time reversal process were discussed. A narrowband excitation was addressed to be advantageous to reduce the frequency dependence of the time reversal operator. Second, the approach of time reversal-based signal enhancement was presented and discussed. The ability of the source focusing based on the time reversal process was adopted to amplify the damage-scattered waves. With the assistance of the time reversal imaging, damage could be well identified. Finally, experiments were conducted to validate the method by ultrasonically examining a quasi-isotropic glass-reinforced epoxy plate. Composite delamination was detected successfully. Further research will investigate the damage evaluation, including damage size, degree and type.

## Acknowledgments

This work is supported by National Natural Science Foundation of China (Grant No. 11202107, 51375414), the Research Fund for the Doctoral Program of Higher Education (Grant No. 20113223120008), the Fundamental Research Funds for the Central Universities (Grant No. NJ20140014) and State Key Laboratory of Mechanics and Control of Mechanical Structures (Nanjing University of Aeronautics and Astronautics) (Grant No. MCMS-0513K01).

## References

Bardos, C. and Fink, M. (2002), "Mathematical foundations of the time reversal mirror", *Asymptotic Anal.*, **29**, 157-182.

Boller, C. (2000), "Next generation structural health monitoring and its integration into aircraft design", *Int. J. Syst. Sci.*, **31**(11), 1333-1349.

Draeger, C., Cassereau, D. and Fink, M. (1997), "Theory of the time-reversal process in solids", *J. Acoust. Soc. Am.*, **102**(3), 1289-1295.

Fink, M. (1999), "Time-reversed acoustics", *Sci. Am.*, **281**(5), 91-97.

Fink, M. and Lewiner, J. (2000), "Method and device for detecting and locating a reflecting sound source", Patent US 6,161,434.

Gangadharan, R., Murthy, C.R.L., Gopalakrishnan, S. and Bhat M.R. (2009), "Time reversal technique for health monitoring of metallic structure using Lamb waves", *Ultrasonics*, **49**, 696-705.

Giurgiutiu, V. (2000), "Active sensors for health monitoring of aging aerospace structures", *Proceedings of the SPIE 7th International Symposium on Smart Structures and Materials and 5th International Symposium on Nondestructive Evaluation and Health Monitoring of Aging Infrastructure*, Newport Beach, California, March.

Ing, R.K. and Fink, M. (1998), "Time reversed Lamb waves", *IEEE T. Ultrason. Ferr.*, **45**(4), 1032-1043.

Jeong, H. (2009), "Time reversal study of ultrasonic waves for anisotropic solids using a Gaussian beam model", *NDT&E Int.*, **42**, 210-214.

Park, H.W., Kim, S.B. and Sohn, H. (2009), "Understanding a time reversal process in Lamb wave propagation", *Wave Motion*, **46**(7), 451-467.

Qiu, L. and Yuan, S. (2009), "On development of a multi-channel PZT array scanning system and its evaluating application on UAV wing box", *Sensor Actuat. A-phys.*, **151**(2), 220-230.

Ratneshwar, J. and Ryan, W. (2009), "Lamb wave based diagnostics of composite plates using modified time reversal method", *Proceedings of the 50th AIAA/ASME/ASCE/AHS/ASC Structures, Structural Dynamics, and Materials Conference*, California, May.

Song, H.C., Hodgkiss, W.S., Kuperman, W.A., Higley, W.J., Raghukumar, K., Akal, T. and Stevenson, M. (2006), "Spatial diversity in passive time reversal communications", *J. Acoust. Soc. Am.*, **120**(4), 2067-2076.

Wang, C.H., Rose, J.T. and Chang, F.K. (2004), "A synthetic time-reversal imaging method for structural health monitoring", *Smart Mater. Struct.*, **13**(2), 415-423.

Xu, B. and Giurgiutiu, V. (2007), "Single mode tuning effects on Lamb wave time reversal with piezoelectric wafer active sensors for structural health monitoring", *J. Nondestruct. Eval.*, **26**(2-4), 123-134.

Yu, L., Bottai-Santoni, G. and Giurgiutiu, V. (2010), "Shear lag solution for tuning ultrasonic piezoelectric wafer active sensors with applications to Lamb wave array imaging", *Int. J. Eng. Sci.*, **48**(10), 848-861.

Yuan, S., Wang, L. and Shi, L. (2003), "On-line damage monitoring in composite structures", *J. Vib. Acoust.*, **125**, 178-186.

Zhang, H., Chen, X., Cao, Y. and Yu, J. (2010), "Focusing of time reversal Lamb waves and its applications in structural health monitoring", *Chinese Phys. Lett*., **27**(10), 104301.

*BS*